Rich nature of the topological semimetal states in InBi

Man Li,[1,*,†] Wenxin Lv,[2,*] Ningning Zhao,[2,*] Chunsheng Gong,[2,3] Tianlun Yu,[4,5] Xiaoyang Chen,[4,5] Minyinan Lei,[4,5] Alexander Fedorov,[6,7,8] Kai Liu,[2] Bernd Büchner,[6,9] Hechang Lei,[2,‡] Shancai Wang,[2] and Rui Lou[6,7,8,*,§]

[1]*School of Information Network Security, People's Public Security University of China, Beijing 100038, China*
[2]*Department of Physics, Key Laboratory of Quantum State Construction and Manipulation (Ministry of Education), and Beijing Key Laboratory of Opto-Electronic Functional Materials & Micronano Devices, Renmin University of China, Beijing 100872, China*
[3]*Beijing Lattice Semiconductor Company Limited, Beijing 101300, China*
[4]*State Key Laboratory of Surface Physics, Department of Physics, and Laboratory of Advanced Materials, Fudan University, Shanghai 200438, China*
[5]*Collaborative Innovation Center of Advanced Microstructures, Nanjing 210093, China*
[6]*Leibniz Institute for Solid State and Materials Research, IFW Dresden, 01069 Dresden, Germany*
[7]*Helmholtz-Zentrum Berlin für Materialien und Energie, Albert-Einstein-Straße 15, 12489 Berlin, Germany*
[8]*Joint Laboratory "Functional Quantum Materials" at BESSY II, 12489 Berlin, Germany*
[9]*Institute for Solid State and Materials Physics, TU Dresden, 01062 Dresden, Germany*

(Received 14 August 2023; revised 28 September 2023; accepted 19 October 2023; published 3 November 2023)

Spin-orbit coupling (SOC) plays a significant role in the development of topological physics. For example, considering the SOC effect would lead to the formation of a topological insulator with band inversion in a time-reversal symmetry-preserved system and the realization of a Chern phase in a time-reversal symmetry-broken system. Here, by using angle-resolved photoemission spectroscopy combined with first-principles electronic structure calculations, we report SOC-induced "hidden" Dirac bands near the Fermi level in the nonsymmorphic topological semimetal InBi. We clearly observe Dirac-like bulk band crossings located at the corner and boundary of the Brillouin zone, providing compelling evidence for three-dimensional Dirac semimetal states. By means of *in situ* potassium dosing on the crystal surface, we are able to reveal a partial Dirac nodal line along the k_z direction formed by Dirac fermions close to the Fermi level. Our results not only demonstrate the rich topological states in InBi but also offer a good platform for engineering topologically nontrivial phases.

DOI: 10.1103/PhysRevB.108.205107

I. INTRODUCTION

Topological materials with exotic band-crossing points protected by symmetry have recently attracted much attention in condensed matter physics. According to the underlying topological properties, the materials hosting these nodes can be classified into topological insulators and topological semimetals [1–4]. In the former, the band crossing is formed by symmetry-protected nontrivial surface states, which can provide unidirectional current to avoid dissipation [5,6], while in the latter, the zero-dimensional nodes of Dirac/Weyl semimetals and the one-dimensional nodes of topological nodal line/ring/link/chain semimetals are associated with the linearly dispersing bulk bands [7–15].

Serving as a fertile ground for topological quantum states and a promising candidate for device applications, topological semimetals have inspired great research interest in the community. Unconventional physical properties usually originate from their band structure with novel quasiparticle excitations near the Fermi level (E_F), such as a large intrinsic spin Hall effect [16], chiral anomaly [17–19], anomalous Hall effect [20,21], as well as novel surface states [7,10,22,23] and the predicted high-temperature superconductivity [24]. Moreover, most of these semimetals also exhibit unusual magnetotransport properties, which are partially due to the linear crossing between the conduction and valence bands with high mobilities and small effective masses, such as the linear transverse magnetoresistance and negative longitudinal magnetoresistance, and more generally, the extremely large transverse magnetoresistance (XMR) in nonmagnetic semimetals [17–19,25–33]. These unsaturated magnetoresistance behaviors have the potential to contribute to the development of spintronics and memory devices.

It has been proposed that the compound of InBi with the nonsymmorphic structure would be an ideal candidate for a nonmagnetic nodal-line semimetal. Furthermore, the nodal-line structures are predicted to be robust against spin-orbit coupling (SOC) due to the protection of the nonsymmorphic symmetry. The nodal lines along the high-symmetry directions of the Brillouin zone (BZ) were previously discovered far below E_F by angle-resolved photoemission spectroscopy (ARPES) measurements [34]. Similar nonsymmorphic symmetry-protected nodal lines have also been reported in the topological semimetals of the ZrSiS family

*These authors contributed equally to this work.
†lmrucphys@ruc.edu.cn
‡hlei@ruc.edu.cn
§lourui09@gmail.com

[35]. Recently, InBi has been found to exhibit XMR behavior and highly anisotropic magnetoresistance in the magnetotransport [36]. According to previous transport measurements and theoretical studies, the observation of field-induced upturn behavior in the resistivity curve and nonsaturating magnetoresistance under high magnetic fields at low temperatures can be attributed to the collaboration between the electron-hole compensation and the linear band dispersions possessing high carrier mobilities in InBi [36,37]. That is to say, there should also exist Dirac-like bands close to E_F in addition to the earlier observed nodal lines far away from E_F. Although near-E_F Dirac band structures of InBi have been theoretically predicted in previous work [36], experimental observations on that topic have not yet been reported. In order to gain insights into the rich topological properties in InBi as well as the origin of the magnetotransport properties, such as XMR, of this compound, an experimental study to reveal its detailed band structure near E_F is desired.

In this paper, we employ systematic ARPES measurements and first-principles calculations to explore the electronic structure of the nonsymmorphic compound InBi. From bulk calculations without including the SOC effect, InBi does not have any Dirac-like band-crossing features near E_F. Once the SOC effect is considered, the Dirac points appear at the BZ boundary and corner. Our ARPES measurements clearly reveal the corresponding bulk band crossings therein, unambiguously demonstrating SOC-induced Dirac semimetal states near E_F in InBi. We then introduce *in situ* electron doping by using a potassium getter, which enables us to observe a partial Dirac nodal line along the k_z direction formed by the Dirac points near E_F. Our results establish InBi as a promising platform for engineering the rich topological states towards realizing additional transport properties.

II. EXPERIMENTS AND CALCULATIONS

Single crystals of InBi were grown by a self-flux technique using In grains (purity 99.9%) and Bi grains (purity 99.9%) with a molar ratio of 11:9. The mixture was put into an alumina crucible and sealed in a quartz ampoule under a partial argon atmosphere. The quartz ampoule was heated up to 573 K for 6 h and held for 6 h. Then it was rapidly cooled down to 473 K in 2 h and slowly cooled down to 373 K. Finally, the InBi single crystals were separated from the flux by a centrifuge. ARPES measurements were performed at the beamline 13U of the National Synchrotron Radiation Laboratory (NSRL), the beamline 5-2 of the Stanford Synchrotron Radiation Lightsource (SSRL), and the Dreamline beamline of the Shanghai Synchrotron Radiation Facility (SSRF) using photons with linear horizontal polarization. The optimal energy and angular resolutions were set to 10 meV and 0.1°, respectively. Samples were cleaved *in situ* along the (001) surface. During the measurements, the temperature was kept at 20 K and the pressure was maintained at better than 5×10^{-11} Torr. First-principles electronic structure calculations on InBi were performed by using the projector augmented-wave (PAW) method [38,39] as implemented in the VASP package [40–42]. The generalized gradient approximation (GGA) of Perdew-Burke-Ernzerhof (PBE) type [43] was used for the exchange-correlation functional. The kinetic energy cutoff of the plane-wave basis was set to 315 eV. The BZ was sampled with a $10 \times 10 \times 10$ k-point mesh. The Gaussian smearing method with a width of 0.05 eV was adopted for the Fermi-surface (FS) broadening.

III. RESULTS AND DISCUSSIONS

As illustrated in Fig. 1(a), InBi crystallizes in a tetragonal structure with the space group $P4/nmm$ (No. 129). The crystal has a layered structure with a natural (001) cleaving plane, due to the relatively weak bonding between the neighboring sublayer of bismuth. The corresponding three-dimensional (3D) bulk and (001)-projected BZs are shown in Fig. 1(b). Figure 1(c) presents an overview of the calculated bulk band structure along the high-symmetry lines for InBi without the SOC effect. There are no linear band-crossing points near E_F herein. When the SOC effect is included in the calculation, one can clearly see the Dirac-like band crossings DP1 and DP2 at the R and M points, respectively, as displayed in Fig. 1(d). To show the characteristics of the Dirac bands more clearly, we present enlarged views of the band crossings in the insets of Fig. 1(d). Meanwhile, no energy gap opens at these Dirac points due to the protection of the nonsymmorphic symmetry in InBi. The core-level photoemission spectrum in Fig. 1(e) shows the characteristic peaks of In-4d and Bi-5d orbitals, further confirming the elemental composition of the sample. In Figs. 1(f) and 1(g), the integrated intensities at $E_F \pm 10$ meV obtained from ARPES measurements in the $k_z \sim 0$ and π planes are shown to represent the FSs, respectively. The fourfold symmetry of the FS mappings is compatible with the tetragonal structure of the (001) surface. We further realize that these two FSs share some similarities, due to the ARPES intensities suffering from the large k_z-broadening effect in a wide vacuum-ultraviolet photon energy range. The strength of k_z broadening, Δk_z, can be roughly evaluated via an equation $\lambda\, \Delta k_z \approx 1$ (λ is the probing depth) that stems from the Heisenberg uncertainty principle. Future studies using the incident photon energies either below 7 eV or in the soft x-ray region are required to effectively reduce the k_z broadening [44–47]. Namely, we have detected the projected ARPES intensity plots containing the information of the electronic states averaged over a finite k_z window, as illustrated in Fig. 1(b).

In order to investigate the Dirac features embedded at the high-symmetry points (R and M), we measure the band structures near E_F along the high-symmetry lines Z-R and Γ-M directions, as indicated by cuts 1 and 2 in Fig. 1(b), respectively. The ARPES intensity plots and the corresponding second derivative intensity plots are illustrated in Figs. 2(a) and 2(b). Along the Z-R direction [Fig. 2(a)], one can clearly see a "W-like" band near E_F forming a Dirac point (DP1) at the R point, which is nearly perfectly aligned with the E_F. Along the Γ-M direction [Fig. 2(b)], we observe that the dispersions around the M point exhibit linearly in a wide energy range ($\sim$1 eV) and form a Dirac point (DP2) at about 0.25 eV below E_F. The Dirac-like crossings of the DP1 and DP2 match well with the superimposed bulk band calculations. The Dirac dispersions of the DP1 and DP2 can be further visualized from the momentum distribution curves (MDCs), as displayed in

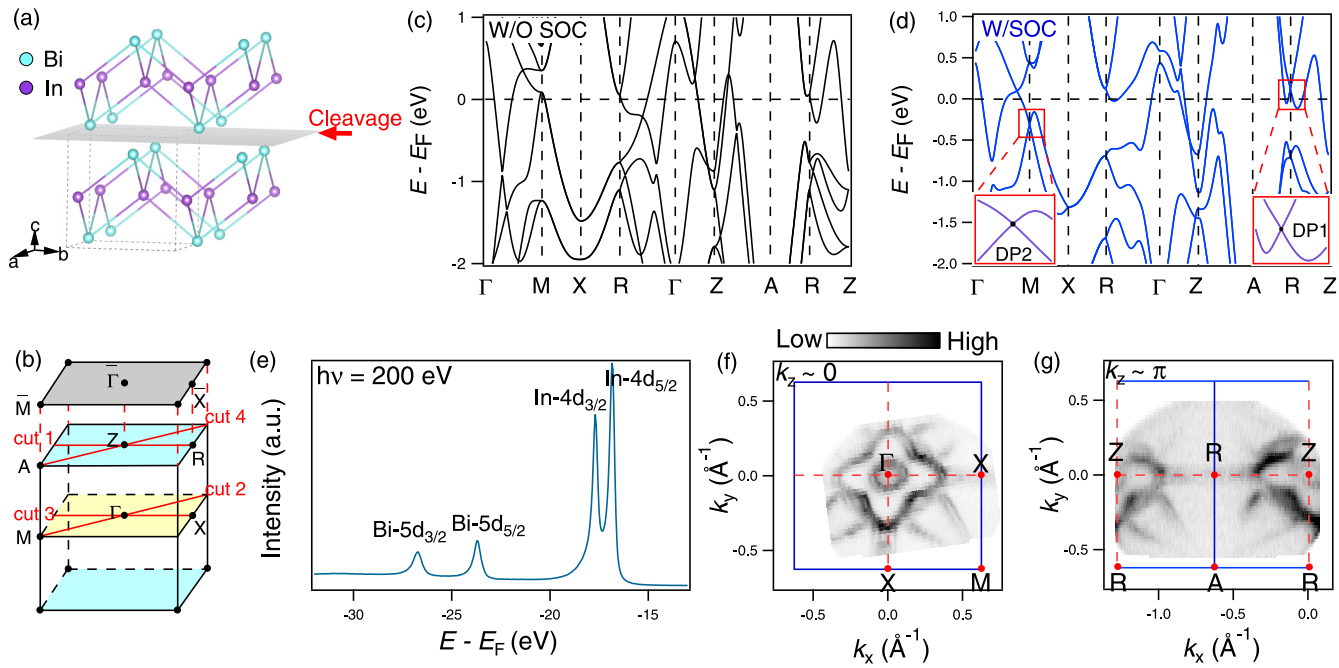

FIG. 1. Crystal structure and electronic structures of InBi. (a) Schematic crystal structure of InBi with space group $P4/nmm$ (No. 129). InBi has a preferred cleaving plane between $InBi_4$-tetrahedron layers. (b) 3D and (001)-projected BZs of InBi with marked high-symmetry points and lines. Cuts 1–4 indicate the locations of the experimental band structures in Fig. 2. (c) Calculated band structure without the SOC effect along high-symmetry lines. (d) Same as (c) with the SOC effect. Insets: Zoomed-in electronic band structure near E_F at the R and M points, respectively. (e) Core-level photoemission spectrum of InBi recorded by 200-eV photons with peaks from each element indicated. (f) Photoemission intensity plot with $h\nu = 17$ eV at E_F measured in the $k_z \sim 0$ plane. (g) Same as (f) measured with $h\nu = 25$ eV in the $k_z \sim \pi$ plane. The blue solid lines in (f) and (g) indicate the (001)-surface BZs.

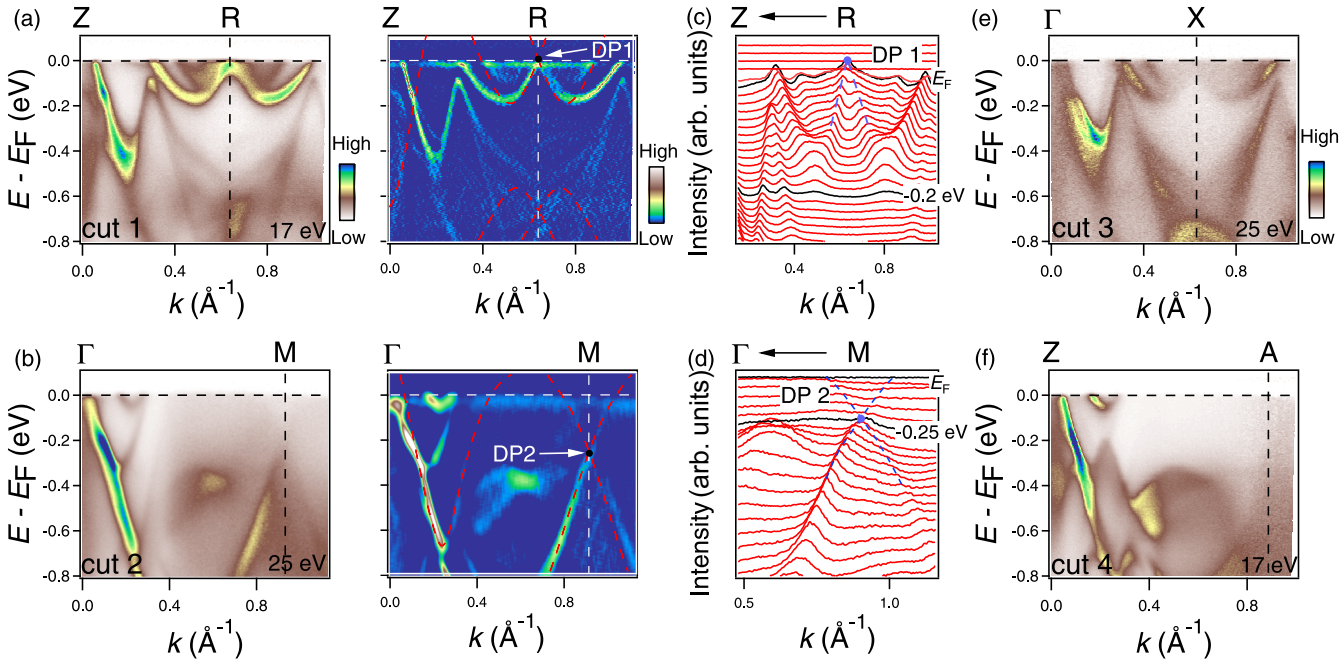

FIG. 2. Near-E_F band structures along high-symmetry lines. (a) Photoemission intensity plot and corresponding second derivative intensity plot along the Z-R direction [cut 1 in Fig. 1(b)]. (b) Same as (a) along the Γ-M direction [cut 2 in Fig. 1(b)]. The appended red solid curves are the bulk band calculations considering the SOC effect. (c), (d) MDC plots around the R and M points, respectively. The blue dashed lines indicate the linear band dispersions. (e), (f) Photoemission intensity plots along the Γ-X and Z-A directions [cuts 3 and 4 in Fig. 1(b)], respectively.

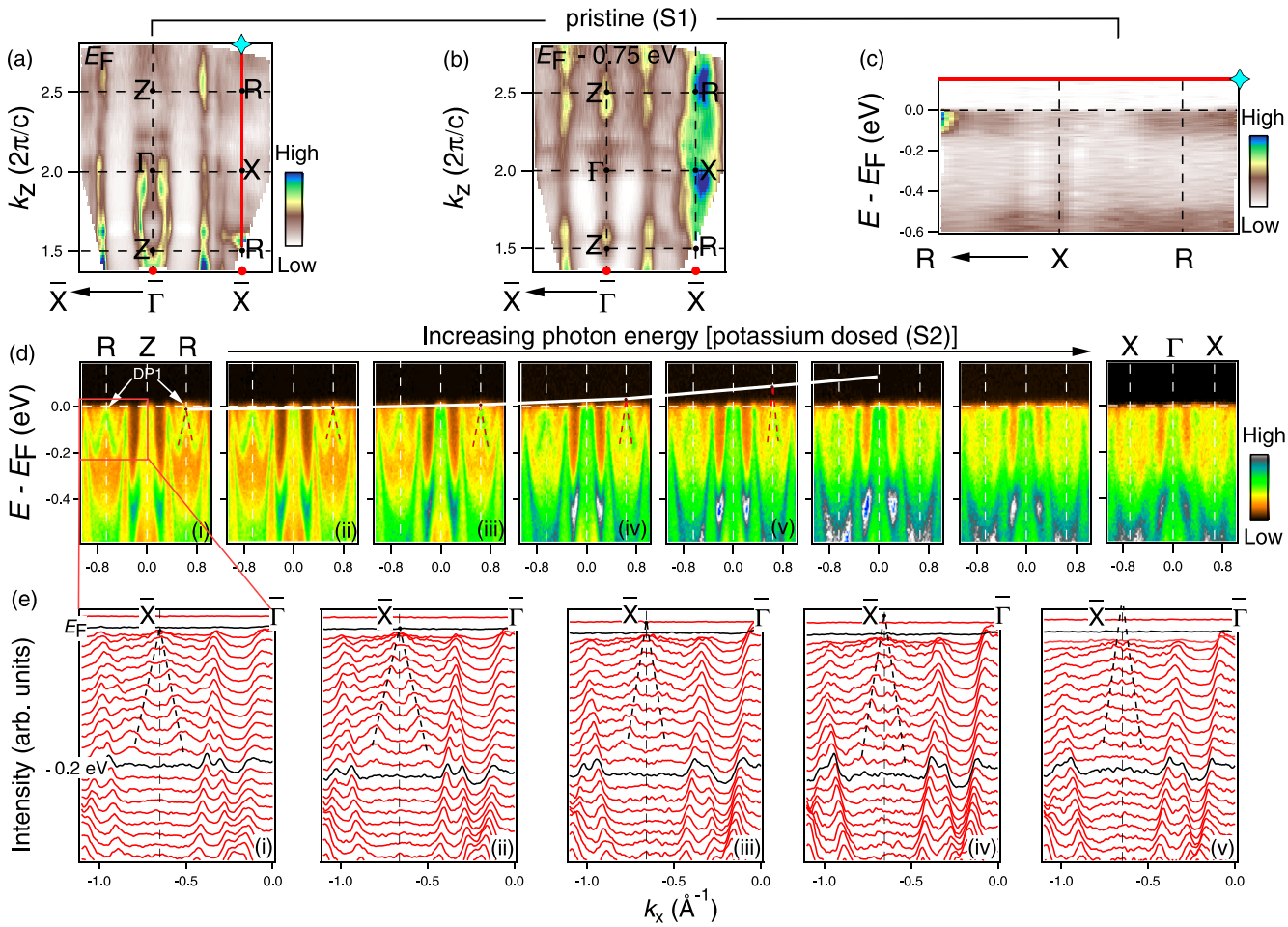

FIG. 3. Photon-energy-dependent measurements of InBi. (a), (b) ARPES intensity plots of the pristine InBi (sample No. 1) in the k_z-$k_\parallel$ plane at E_F and 0.75 eV below E_F with $k_\parallel$ oriented along the $\bar{\Gamma}$-$\bar{X}$ direction, respectively. (c) Intensity plot of pristine InBi taken along the X-R direction, as indicated by the red solid line in (a). (d) Photoemission intensity plots measured with variable photon energies along the $\bar{X}$-$\bar{\Gamma}$-$\bar{X}$ line after potassium dosing on sample No. 2, where DP1 sinks below E_F at the R point (leftmost panel). The appended red dashed lines are guides to the eye for the linear band crossings. The Dirac nodal line is indicated by the white solid curve. (e) MDC plots of (d)(i)–(d)(v). The momentum range is indicated by the red solid rectangle in (d). The black dashes indicate the linear bands forming DP1.

Figs. 2(c) and 2(d), respectively. To confirm the 3D characteristics of these Dirac points, we present the ARPES spectra along the Γ-X and Z-A lines [indicated by cuts 3 and 4 in Fig. 1(b)] in Figs. 2(e) and 2(f), respectively. One can obtain that, although the k_z-broadening effect is still present around the Γ and Z points, there is no evident signature of linear band dispersions near E_F at the X and A points, in contrast to that at the R and M points. Therefore, we unambiguously demonstrate the existence of SOC-induced 3D Dirac fermions near E_F. We also notice that some experimental band dispersions near the Γ, Z, and R points are not reproduced by the bulk calculations. These bands most likely come from the contributions of the bulk states projected from other k_z planes due to the k_z-broadening effect as well as the surface states [34,44,46,47]. It should be noted that the observed W-like band around the R point [Fig. 2(a)] is actually contributed by both the states in the bulk and on the surface—the inner part forming the DP1 at E_F comes from the states in the bulk, while the outer part which is not reproduced by the bulk calculations comes from the states on the topmost several layers of the crystal, as suggested by earlier slab model calculations [34]. Future bulk-sensitive soft x-ray ARPES measurements are desired to avoid possible interference from these states on the crystal surface.

Then, we perform the k_z-dependent measurements by varying the photon energies from 13 to 39 eV, which covers more than one BZ along the k_z direction. Figures 3(a) and 3(b) show the ARPES intensity plots at E_F and 0.75 eV below E_F as a function of the photon energy (i.e., the k_z) and the in-plane momentum, which is oriented along the $\bar{\Gamma}$-$\bar{X}$ direction. One can clearly observe that the photoemission intensities exhibit periodic modulations along the Γ-Z and X-R lines, validating the assignment of the k_z values in our work. We then present the band dispersions taken along the X-R direction in Fig. 3(c). One can clearly see the difference between the X and R points. The intensity from the Dirac band near E_F is observable at the R point, in contrast to that around the X point. This modulation is compatible with the k_z-$k_\parallel$ mappings in Figs. 2(a) and 2(b), again validating the 3D character of the Dirac-like dispersions around the R point.

Based on the observations presented above, we have successfully realized the low-energy Dirac quasiparticle excitations in InBi. In particular, the Dirac quasiparticle at the R point, which is nearly perfectly aligned with E_F, is expected to make a non-negligible contribution to the transport properties. In order to examine its tunability for future spintronic applications, we now deposit potassium on a freshly cleaved InBi crystal (sample No. 2). The resulting band structures and corresponding MDC plots along the $\bar{\Gamma}$-$\bar{X}$ directions are presented in Figs. 3(d) and 3(e). One obtains that the linear bands cross each other forming a Dirac point (DP1) slightly below E_F (∼20 meV) in Figs. 3(d)(i) and 3(e)(i), while for the pristine sample [Figs. 2(a) and 2(c), sample No. 1], the DP1 is located exactly at E_F. Although the current data of the pristine and K-dosed InBi are not from the same sample, our observations still show that alkali-metal deposition is a promising way to tune the Dirac points in InBi. By increasing the incident photon energy, we reveal that the DP1 at the R point gradually moves upwards in energy [Figs. 3(d)(i)–(v) and 3(e)(i)–(v)], behaving as the Dirac nodal line predicted by earlier calculations [34], as guided by the white solid curve in Fig. 3(d). This nodal line has been theoretically predicted to lie completely above E_F along the X-R direction [34]. Now we may have successfully tuned it slightly below E_F, at least partially. It is noted that the bands around the $\bar{X}$ point become smeared at a higher photon energy [Fig. 3(d)]. We speculate that this could be due to the Dirac nodal line dispersing fast along the X-R direction, thus the corresponding linear bands are located completely above E_F. Both the observed 3D Dirac fermions and the partial Dirac nodal line are close to E_F, suggesting that the low-energy quasiparticle excitations of InBi are drastically different from the usual Schrödinger-type fermions, and thus may make a contribution to the underlying XMR behavior together with the electron-hole compensation [36,37].

IV. CONCLUSION

In summary, we have studied the electronic structure of the topological semimetal InBi by ARPES experiments and first-principles calculations. Our results suggest that the SOC-induced 3D Dirac fermions are realized at the BZ boundary and corner (R and M points, respectively). By means of *in situ* potassium deposition, we are able to observe a partial Dirac nodal line along the k_z direction (X-R line) constituted by the near-E_F Dirac fermions. Our study suggests that InBi serves as a good playground for engineering the topological properties and exploring the relationship between the magnetotransport phenomena and the band topology.

ACKNOWLEDGMENTS

The authors acknowledge Donglai Feng for helpful discussions. In addition, we acknowledge Makoto Hashimoto and Donghui Lu for assisting with the ARPES measurements at SSRL. This work was supported by the National Natural Science Foundation of China (Grants No. 12204536 and No. 11904144), the Deutsche Forschungsgemeinschaft under Grant SFB 1143 (project C04), the Würzburg-Dresden Cluster of Excellence on Complexity and Topology in Quantum Matter – *ct.qmat* (EXC 2147, project ID 390858490), the Fundamental Research Funds for the Central Universities, and the Research Funds of People's Public Security University of China (PPSUC) (2023JKF02ZK09). B.B. acknowledges the support from the BMBF via project UKRATOP. H.C.L. was supported by the National Key R&D Program of China (Grants No. 2018YFE0202600 and No. 2022YFA1403800), the Beijing Natural Science Foundation (Grant No. Z200005), and the National Natural Science Foundation of China (Grant No. 12174443).

[1] A. Bansil, H. Lin, and T. Das, Colloquium: Topological band theory, Rev. Mod. Phys. **88**, 021004 (2016).

[2] N. P. Armitage, E. J. Mele, and A. Vishwanath, Weyl and Dirac semimetals in three-dimensional solids, Rev. Mod. Phys. **90**, 015001 (2018).

[3] J. A. Sobota, Y. He, and Z.-X. Shen, Angle-resolved photoemission studies of quantum materials, Rev. Mod. Phys. **93**, 025006 (2021).

[4] B. Q. Lv, T. Qian, and H. Ding, Experimental perspective on three-dimensional topological semimetals, Rev. Mod. Phys. **93**, 025002 (2021).

[5] J. E. Moore, The birth of topological insulators, Nature (London) **464**, 194 (2010).

[6] X.-L. Qi and S.-C. Zhang, Topological insulators and superconductors, Rev. Mod. Phys. **83**, 1057 (2011).

[7] Z. K. Liu, B. Zhou, Y. Zhang, Z. J. Wang, H. M. Weng, D. Prabhakaran, S.-K. Mo, Z. X. Shen, Z. Fang, X. Dai, Z. Hussain, and Y. L. Chen, Discovery of a three-dimensional topological Dirac semimetal, Na_3Bi, Science **343**, 864 (2014).

[8] S. Borisenko, Q. Gibson, D. Evtushinsky, V. Zabolotnyy, B. Büchner, and R. J. Cava, Experimental realization of a three-dimensional Dirac semimetal, Phys. Rev. Lett. **113**, 027603 (2014).

[9] S.-Y. Xu, I. Belopolski, N. Alidoust, M. Neupane, G. Bian, C. Zhang, R. Sankar, G. Chang, Z. Yuan, C.-C. Lee, S.-M. Huang, H. Zheng, J. Ma, D. S. Sanchez, B. Wang, A. Bansil, F. Chou, P. P. Shibayev, H. Lin, S. Jia, and M. Z. Hasan, Discovery of a Weyl fermion semimetal and topological Fermi arcs, Science **349**, 613 (2015).

[10] B. Q. Lv, S. Muff, T. Qian, Z. D. Song, S. M. Nie, N. Xu, P. Richard, C. E. Matt, N. C. Plumb, L. X. Zhao, G. F. Chen, Z. Fang, X. Dai, J. H. Dil, J. Mesot, M. Shi, H. M. Weng, and H. Ding, Observation of Fermi-arc spin texture in TaAs, Phys. Rev. Lett. **115**, 217601 (2015).

[11] D. F. Liu, A. J. Liang, E. K. Liu, Q. N. Xu, Y. W. Li, C. Chen, D. Pei, W. J. Shi, S. K. Mo, P. Dudin, T. Kim, C. Cacho, G. Li, Y. Sun, L. X. Yang, Z. K. Liu, S. S. P. Parkin, C. Felser, and Y. L. Chen, Magnetic Weyl semimetal phase in a kagome crystal, Science **365**, 1282 (2019).

[12] L. M. Schoop, M. N. Ali, C. Straßer, A. Topp, A. Varykhalov, D. Marchenko, V. Duppel, S. S. P. Parkin, B. V. Lotsch, and C. R. Ast, Dirac cone protected by non-symmorphic symmetry and three-dimensional Dirac line node in ZrSiS, Nat. Commun. **7**, 11696 (2016).

[13] Z. Yan, R. Bi, H. Shen, L. Lu, S.-C. Zhang, and Z. Wang, Nodal-link semimetals, Phys. Rev. B **96**, 041103(R) (2017).

[14] T. Bzdušek, Q. Wu, A. Røuegg, M. Sigrist, and A. A. Soluyanov, Nodal-chain metals, Nature (London) **538**, 75 (2016).

[15] C. Song, L. Jin, P. Song, H. Rong, W. Zhu, B. Liang, S. Cui, Z. Sun, L. Zhao, Y. Shi, X. Zhang, G. Liu, and X. J. Zhou, Spectroscopic evidence for Dirac nodal surfaces and nodal rings in the superconductor NaAlSi, Phys. Rev. B **105**, L161104 (2022).

[16] Y. Sun, Y. Zhang, C. Felser, and B. Yan, Strong intrinsic spin Hall effect in the TaAs family of Weyl semimetals, Phys. Rev. Lett. **117**, 146403 (2016).

[17] X. Huang, L. Zhao, Y. Long, P. Wang, D. Chen, Z. Yang, H. Liang, M. Xue, H. Weng, Z. Fang, X. Dai, and G. Chen, Observation of the chiral-anomaly-induced negative magnetoresistance in 3D Weyl semimetal TaAs, Phys. Rev. X **5**, 031023 (2015).

[18] C.-L. Zhang, S.-Y. Xu, I. Belopolski, Z. Yuan, Z. Lin, B. Tong, G. Bian, N. Alidoust, C.-C. Lee, S.-M. Huang, T.-R. Chang, G. Chang, C.-H. Hsu, H.-T. Jeng, M. Neupane, D. S. Sanchez, H. Zheng, J. Wang, H. Lin, C. Zhang, H.-Z. Lu, S.-Q. Shen, T. Neupert, M. Z. Hasan, and S. Jia, Signatures of the Adler-Bell-Jackiw chiral anomaly in a Weyl fermion semimetal, Nat. Commun. **7**, 10735 (2016).

[19] C.-Z. Li, L.-X. Wang, H. Liu, J. Wang, Z.-M. Liao, and D.-P. Yu, Giant negative magnetoresistance induced by the chiral anomaly in individual Cd_3As_2 nanowires, Nat. Commun. **6**, 10137 (2015).

[20] T. Liang, J. Lin, Q. Gibson, S. Kushwaha, M. Liu, W. Wang, H. Xiong, J. A. Sobota, M. Hashimoto, P. S. Kirchmann, Z.-X. Shen, R. J. Cava, and N. P. Ong, Anomalous Hall effect in $ZrTe_5$, Nat. Phys. **14**, 451 (2018).

[21] E. Liu, Y. Sun, N. Kumar, L. Muechler, A. Sun, L. Jiao, S.-Y. Yang, D. Liu, A. Liang, Q. Xu, J. Kroder, V. Süß, H. Borrmann, C. Shekhar, Z. Wang, C. Xi, W. Wang, W. Schnelle, S. Wirth, Y. Chen, S. T. B. Goennenwein, and C. Felser, Giant anomalous Hall effect in a ferromagnetic kagome-lattice semimetal, Nat. Phys. **14**, 1125 (2018).

[22] S.-M. Huang, S.-Y. Xu, I. Belopolski, C.-C. Lee, G. Chang, B. Wang, N. Alidoust, G. Bian, M. Neupane, C. Zhang, S. Jia, A. Bansil, H. Lin, and M. Z. Hasan, A Weyl fermion semimetal with surface Fermi arcs in the transition metal monopnictide TaAs class, Nat. Commun. **6**, 7373 (2015).

[23] G. Bian, T.-R. Chang, R. Sankar, S.-Y. Xu, H. Zheng, T. Neupert, C.-K. Chiu, S.-M. Huang, G. Chang, I. Belopolski, D. S. Sanchez, M. Neupane, N. Alidoust, C. Liu, B. Wang, C.-C. Lee, H.-T. Jeng, C. Zhang, Z. Yuan, S. Jia, A. Bansil, F. Chou, H. Lin, and M. Z. Hasan, Topological nodal-line fermions in spin-orbit metal $PbTaSe_2$, Nat. Commun. **7**, 10556 (2016).

[24] N. B. Kopnin, T. T. Heikkilä, and G. E. Volovik, High-temperature surface superconductivity in topological flat-band systems, Phys. Rev. B **83**, 220503(R) (2011).

[25] J. Xiong, S. K. Kushwaha, T. Liang, J. W. Krizan, M. Hirschberger, W. Wang, R. J. Cava, and N. P. Ong, Evidence for the chiral anomaly in the Dirac semimetal Na_3Bi, Science **350**, 413 (2015).

[26] L. X. Yang, Z. K. Liu, Y. Sun, H. Peng, H. F. Yang, T. Zhang, B. Zhou, Y. Zhang, Y. F. Guo, M. Rahn, D. Prabhakaran, Z. Hussain, S.-K. Mo, C. Felser, B. Yan, and Y. L. Chen, Weyl semimetal phase in the non-centrosymmetric compound TaAs, Nat. Phys. **11**, 728 (2015).

[27] J. Feng, Y. Pang, D. Wu, Z. Wang, H. Weng, J. Li, X. Dai, Z. Fang, Y. Shi, and L. Lu, Large linear magnetoresistance in Dirac semimetal Cd_3As_2 with Fermi surfaces close to the Dirac points, Phys. Rev. B **92**, 081306(R) (2015).

[28] T. Liang, Q. Gibson, M. N. Ali, M. Liu, R. J. Cava, and N. P. Ong, Ultrahigh mobility and giant magnetoresistance in the Dirac semimetal Cd_3As_2, Nat. Mater. **14**, 280 (2015).

[29] E. Mun, H. Ko, G. J. Miller, G. D. Samolyuk, S. L. Bud'ko, and P. C. Canfield, Magnetic field effects on transport properties of $PtSn_4$, Phys. Rev. B **85**, 035135 (2012).

[30] R. Xu, A. Husmann, T. F. Rosenbaum, M.-L. Saboungi, J. E. Enderby, and P. B. Littlewood, Large magnetoresistance in non-magnetic silver chalcogenides, Nature (London) **390**, 57 (1997).

[31] H. Li, H. He, H.-Z. Lu, H. Zhang, H. Liu, R. Ma, Z. Fan, S.-Q. Shen, and J. Wang, Negative magnetoresistance in Dirac semimetal Cd_3As_2, Nat. Commun. **7**, 10301 (2016).

[32] S. Li, Z. Guo, D. Fu, X.-C. Pan, J. Wang, K. Ran, S. Bao, Z. Ma, Z. Cai, R. Wang, R. Yu, J. Sun, F. Song, and J. Wen, Evidence for a Dirac nodal-line semimetal in $SrAs_3$, Sci. Bull. **63**, 535 (2018).

[33] C. Shekhar, A. K. Nayak, Y. Sun, M. Schmidt, M. Nicklas, I. Leermakers, U. Zeitler, Y. Skourski, J. Wosnitza, Z. Liu, Y. Chen, W. Schnelle, H. Borrmann, Y. Grin, C. Felser, and B. Yan, Extremely large magnetoresistance and ultrahigh mobility in the topological Weyl semimetal candidate NbP, Nat. Phys. **11**, 645 (2015).

[34] S. A. Ekahana, S.-C. Wu, J. Jiang, K. Okawa, D. Prabhakaran, C.-C. Hwang, S.-K. Mo, T. Sasagawa, C. Felser, B. Yan, Z. Liu, and Y. Chen, Observation of nodal line in non-symmorphic topological semimetal InBi, New J. Phys. **19**, 065007 (2017).

[35] B.-B. Fu, C.-J. Yi, T.-T. Zhang, M. Caputo, J.-Z. Ma, X. Gao, B. Q. Lv, L.-Y. Kong, Y.-B. Huang, P. Richard, M. Shi, V. N. Strocov, C. Fang, H.-M. Weng, Y.-G. Shi, T. Qian, and H. Ding, Dirac nodal surfaces and nodal lines in ZrSiS, Sci. Adv. **5**, eaau6459 (2019).

[36] K. Okawa, M. Kanou, H. Namiki, and T. Sasagawa, Extremely large magnetoresistance induced by hidden three-dimensional Dirac bands in nonmagnetic semimetal InBi, Phys. Rev. Mater. **2**, 124201 (2018).

[37] S. Dan, K. Kargeti, R. C. Sahoo, S. Dan, D. Pal, S. Verma, S. Chakravarty, S. K. Panda, and S. Patil, Magnetotransport properties and Fermi surface topology of the nodal line semimetal InBi, Phys. Rev. B **107**, 205111 (2023).

[38] P. E. Blöchl, Projector augmented-wave method, Phys. Rev. B **50**, 17953 (1994).

[39] G. Kresse and D. Joubert, From ultrasoft pseudopotentials to the projector augmented-wave method, Phys. Rev. B **59**, 1758 (1999).

[40] G. Kresse and J. Hafner, *Ab initio* molecular dynamics for liquid metals, Phys. Rev. B **47**, 558 (1993).

[41] G. Kresse and J. Furthmüller, Efficiency of *ab-initio* total energy calculations for metals and semiconductors using a plane-wave basis set, Comput. Mater. Sci. **6**, 15 (1996).

[42] G. Kresse and J. Furthmüller, Efficient iterative schemes for *ab initio* total-energy calculations using a plane-wave basis set, Phys. Rev. B **54**, 11169 (1996).

[43] J. P. Perdew, K. Burke, and M. Ernzerhof, Generalized gradient approximation made simple, Phys. Rev. Lett. **77**, 3865 (1996).

[44] H. Zhang, T. Pincelli, C. Jozwiak, T. Kondo, R. Ernstorfer, T. Sato, and S. Zhou, Angle-resolved photoemission spectroscopy, Nat. Rev. Methods Primers **2**, 54 (2022).

[45] M. P. Seah and W. A. Dench, Quantitative electron spectroscopy of surfaces: A standard data base for electron inelastic mean free paths in solids, Surf. Interface Anal. **1**, 2 (1979).

[46] R. L. Kurtz, D. A. Browne, and G. J. Mankey, Final state effects in photoemission studies of Fermi surfaces, J. Phys.: Condens. Matter **19**, 355001 (2007).

[47] V. N. Strocov, Intrinsic accuracy in 3-dimensional photoemission band mapping, J. Electron Spectrosc. Relat. Phenom. **130**, 65 (2003).